Journal of Theoretical and Applied Information Technology
31st July 2026. Vol.104. No.14

ISSN: 1992-8645 www.jatit.org E-ISSN: 1817-3195

DUAL-WAY F2M3SLNN: MRI AND PET MULTI-MODALITY FUSION BASED BRAIN TUMOR DIAGNOSIS USING PALE STRUCTURED TRANSFORMER AND SKIP CONNECTED LSTM

SANTHOSH KUMAR. S[1], DR. S.P.SASIREKHA[2], DR.R.SANTHOSH[3]

[1]Research scholar. Department of Computer Science and Engineering, Faculty of Engineering, Karpagam Academy of Higher Education, Coimbatore, Tamil Nadu, India
[2]Assistant Professor, Department of Computer Science and Engineering, Faculty of Engineering, Karpagam Academy of Higher Education, Coimbatore, Tamil Nadu, India
[3]Professor and Head, Department of Computer Science and Engineering, Faculty of Engineering, Karpagam Academy of Higher Education, Coimbatore, Tamil Nadu, India.

E-mail:[1]santhoshkumars@myyahoo.com, [2]csrd411@gmail.com, [3]cyberphd85@gmail.com

ABSTRACT

A brain tumor signifies an irregular proliferation of cells that replicate uncontrollably. Within a medical diagnostic system, the precise identification of both the location and size assumes a critical role in brain tumor diagnosis. The primary diagnostic modalities for this purpose encompass Magnetic Resonance Imaging (MRI) and Positron Emission Tomography (PET), both being extensively employed techniques. Identifying brain tumors in PET and MRI images presents a formidable challenge, primarily stemming from the low sensitivity of boundary pixels. To achieve precise and reliable brain tumor detection, the recent studies introduces an efficient fusion-based approach in its methodology however it declines to provide accurate results. To alleviate these issues, we have proposed multi-modality based brain tumor classification named as Dual-way F^2M^3 SLNN framework. Initially, for utilizing both MRI and PET information we have performed Multi-modality image fusion by proposing TangleNet via Average Norm Technique (ANT). After that, we have enhanced fused image quality by executing pre-processing in terms of noise reduction and bias field correction using Quaternion Quasi-Chebyshev with Non-Local Means (QQC-NLM) and Expectation Maximization respectively. Besides, the pre-processed image quality is ensured by performing image quality evaluation using Kernel Support Vector Machine (K-SVM). Following that, the appropriate features are extracted by Pale structure transformer and feature dimension are reduced through employing Analogous Attention Mechanism. Finally, the accurate brain tumor is classified using Skip connected Long Short-Term Memory (SC-LSTM). The proposed Dual-way F^2M^3 SLNN framework is conducted on MATLAB for improving model performance, additionally the performance of proposed model is evaluated by determining several performance metrics in terms of accuracy, sensitivity, specificity, F1-Score and AUC where our proposed Dual-way F^2M^3 SLNN framework achieves superior achievement than other existing works.

Keywords –*Multi-modality, Image Fusion, Brain Tumor Classification, MRI & PET, Pale Structured Transformer, Analogous Attention Mechanism.*

1. INTRODUCTION

Primary central nervous system tumors exhibit one of the highest cancer incidence rates among patients of all ages, with nearly 400,000 cases reported in the United States between 2012 and 2016 [1]. Of these cases, over two-thirds are classified as benign, while the remaining malignant tumors significantly contribute to morbidity and mortality [2]. Secondary brain tumors, including brain metastases, are ten times more prevalent and exert a substantial impact on outcome data. Despite notable progress in the management of brain tumor patients, high-grade malignancies

remain challenging to treat. For example, patients with glioblastoma (GBM) have a life expectancy of approximately 20 months, even with the addition of tumor-treating fields to the standard care regimen [3]. In a broader context, only 23.5% of patients with malignant brain or spine tumors are expected to survive beyond 5 years, based on data compiled from the Central Brain Tumor Registry spanning the years 2013 to 2017 [4][5].

Basically, human brain, a marvel of complexity, operates through billions of cells [6]. When a cluster of abnormal cells develops within or around the brain, it gives rise to a brain tumor. These cells can disrupt normal brain function and harm healthy ones. Detecting brain tumors in their early stages is pivotal, circumventing the time-consuming manual segmentation of extensive datasets [7]-[9]. The existence of various distinct types of brain tumors adds complexity to their identification. Hence, categorizing the specific type of brain tumor afflicting a patient holds great significance. An effective classification process leads to informed decisions and facilitates appropriate treatment [10]-[12]. Typically, early-stage brain tumor assessments involve various diagnostic techniques such as scans, nerve tests, X-rays, and biopsies. Presently, with the rapid advancements in artificial intelligence (AI) and biomedical progress, computer-aided diagnoses, PET scans, and MRI scans have garnered increased attention [13][14]. These global brain imaging technologies offer invaluable insights to physicians and researchers regarding both normal and abnormal brain tissue. MRI, employing magnetic fields, is adept at detecting changes within the brain and delivers high-quality results. In contrast, PET scans utilize radiation to identify tissue abnormalities. Notably, MRI stands out for its non-harmful impact on human health [15].

Dimensionality reduction and feature selection play crucial roles in tumor classification [16][17]. Contemporary tools and methodologies for analysing tumors and their behavior have gained increased prominence. Image processing techniques can effectively identify brain tumors by converting images into digital format and applying operations to enhance their quality [18]. Analysing brain tumors poses challenges due to their diverse shapes, sizes, locations, and variations in appearance within the brain. Detecting brain tumors in their early stages is challenging because accurate measurements are elusive [19][20]. However, early detection of brain tumors opens the door to potential curative treatments. Currently, medical imaging techniques provide visual representations of the body's interior for clinical analysis and medical research purposes.

1.1. Motivation

In contemporary times, one of the leading causes of increased mortality among both children and adults is brain tumors. Research conducted in most developed countries reveals a significant rise in the number of individuals suffering from and succumbing to brain tumors, with an annual increase of up to 300 cases over recent decades. The National Brain Tumor Foundation (NBTF) for research in the United States estimates that 13,000 patients lose their lives, while 29,000 receive a primary brain tumor diagnosis each year. This alarming mortality rate underscores the critical importance of effective brain tumor detection. The primary challenge in tumor detection arises from the inherent variability in tumor characteristics, such as shape, size, location, and intensity. Manual tumor detection relies on human intervention and is a time-consuming process, heavily reliant on the observer's ability to discern these tumor attributes. Understanding the impact of brain tumors necessitates a comprehensive knowledge of the functions of each part of the brain.

In recent developments in medical imaging, real-time tumor diagnosis using more dependable algorithms has become a central focus. Detecting brain tumors in MRI and PET scan images has emerged as an active area of research. Among the challenges faced by medical imaging diagnosis systems, the separation of cells and their nuclei from the rest of the image content stands out as a primary concern. This critical process, known as segmentation, holds paramount importance in building a robust diagnosis system. Image classification is carried out on input images, facilitating a more accessible analysis of the image and ultimately enhancing tumor detection efficiency. Consequently, image classification forms the foundational challenge in the realm of tumor detection.

1.2. Research Contribution

The main contribution of our proposed Dual-way F^2M^3 SLNN framework is to diagnosis accurate brain tumor classification. To attain appropriate results we have proposed several contribution in our work which are articulated as below,

- The proposed approach leverages multi-modality image fusion techniques,

specifically utilizing both MRI and PET information. This integration enhances the comprehensiveness of the data used for diagnosis.

- Framework incorporates advanced pre-processing techniques, including noise reduction and bias field correction. These steps are vital for enhancing the quality of the fused images, thereby improving the accuracy of tumor detection.
- To ensure the quality of the pre-processed images, the study conducts image quality evaluation using Kernel Support Vector Machine (K-SVM). This step helps in validating the effectiveness of the image enhancement process.
- The framework introduces innovative methods for feature extraction using the Pale structure transformer and feature dimension reduction through the Analogous Attention Mechanism. Additionally, accurate brain tumor classification is achieved using Skip connected Long Short-Term Memory (SC-LSTM), contributing to the overall precision of the system.

1.3. Paper Organization

The paper is structured as follows: In Section II, we delve into prior research on brain tumor classification. Section III offers a comprehensive explanation of the research methodology of proposed Dual-way F^2M^3 SLNN framework, complete with relevant mathematical equations, pseudocode, and diagrams. Moving on to Section IV, we provide a concise overview of the experimental results, encompassing dataset descriptions and comparative analyses. Section V focuses on discussing the outcomes of our proposed approach, and finally, in Section VI, we draw conclusions from our research work.

2. LITERATURE SURVEY

Preethi et al. [21] introduces a novel approach for detecting and segmenting brain tumors using a wavelet-based image fusion technique applied to both PET and MRI images. The fusion of these two modalities allows for a more comprehensive and accurate assessment of brain tumors. The paper emphasizes the importance of multi-modal imaging in brain tumor diagnosis and highlights the potential of wavelet-based fusion and utilize optimal deep neural network (ODNN) for brain tumor classification. Overcast et al. [22] reviews advanced imaging techniques for the diagnosis of neuro-oncologic tumors, with a specific focus on the combination of PET and MRI imaging for detecting malignant brain tumors. It provides insights into the benefits and challenges of using PET-MRI fusion in clinical practice and its potential to improve the accuracy of brain tumor diagnosis. The paper contributes to the understanding of cutting-edge neuro-oncologic imaging methods. Ramprasad et al. [23] proposes a deep learning model that integrates Fusion-Net architecture with HFCMIK segmentation for brain tumor classification. It introduces a probabilistic sensing and learning approach, emphasizing the significance of probabilistic modeling in improving brain tumor classification accuracy by utilizing deep learning based probabilistic neural network (DLPNN). Ahmad et al. [24] explores the application of generative adversarial networks (GANs) and variational autoencoders (VAEs) in the classification of brain tumors. By combining these two innovative techniques, the research aims to improve the accuracy of tumor classification. The paper underscores the role of generative models in extracting meaningful features for classification tasks in medical imaging. Kang et al. [25] focuses on the classification of brain tumors using MRI images and an ensemble of deep features combined with machine learning classifiers. It highlights the significance of feature engineering and ensemble methods in improving the accuracy of tumor classification based on MRI data in which support vector machine (SVM) with radial basis function (RBF) executes effectively.

Nawaz et al. [26] delves into brain tumor classification using a hybrid approach that optimizes multi-feature analysis applied to Magnetic Resonance Imaging (MRI) datasets. It emphasizes the importance of feature engineering and optimization techniques to enhance the accuracy of brain tumor classification based on MRI data. Yadav et al. [27] introduces a novel approach for feature extraction in brain tumor classification, leveraging Probabilistic Neural Networks and the BTFSC-Net model. It underscores the significance of combining deep learning and probabilistic methods to improve the accuracy of classification tasks in brain tumor diagnosis. Ahuja et al. [28] explores the utilization of Dark-Nets, a variant of deep neural networks, for brain tumor classification and segmentation. It highlights the improved performance achieved through the incorporation of colormap-based super-pixel techniques, demonstrating the potential of advanced neural networks in medical imaging

tasks. Amin et al. [29] focuses on brain tumor classification by fusing Discrete Wavelet Transform (DWT) features extracted from MRI sequences with a Convolutional Neural Network (CNN) architecture. It illustrates the advantages of integrating signal processing techniques with deep learning for accurate brain tumor classification. Aamir et al. [30] presents a deep learning approach for the classification of brain tumors using MRI images. It underscores the potential of deep neural networks in automatically extracting meaningful features from MRI data, leading to improved accuracy in brain tumor classification.

Amin et al. [31] presents a unique approach to brain tumor detection and classification utilizing Magnetic Resonance Imaging (MRI). It explores innovative methods for extracting relevant features from MRI data to improve the accuracy of tumor detection and classification. This paper contributes to the ongoing efforts to enhance brain tumor diagnosis through advanced MRI-based techniques. Muezzinoglu et al. [32] introduces a novel framework called PatchResNet, which is centred around multiple patch divisions for deep feature fusion in brain tumor classification. It demonstrates how dividing the image into patches and fusing their features can enhance the performance of classification models. Sharif et al. [33] paper presents an enhanced framework for analyzing brain tumors in MRI images by incorporating the YOLOv2 (You Only Look Once) object detection model and convolutional neural networks (CNNs). By integrating these cutting-edge techniques, the paper aims to improve the efficiency and accuracy of brain tumor analysis based on MRI data. Tandel et al. [34] addresses the challenge of multiclass brain tumor classification using Magnetic Resonance Imaging (MRI) and artificial intelligence techniques. It explores the application of AI algorithms to categorize brain tumors into multiple classes, contributing to a more comprehensive understanding of tumor types and their characteristics. Aamir et al. [35] focuses on brain tumor classification by leveraging deep features extracted from high-quality regions within MRI images. It emphasizes the importance of identifying and utilizing specific image regions that provide the most informative data for accurate classification.

Kolla et al. [36] presents a brain tumor detection model that leverages Convolutional Neural Networks (CNNs) along with Local Binary Pattern (LBP) features and a multilayered Support Vector Machine (SVM) classifier. The combination of CNN for feature extraction and LBP for texture analysis enhances the accuracy of brain tumor detection. Nayan et al. [37] introduces a deep learning-based approach for detecting brain tumors using Magnetic Resonance Imaging (MRI) scans. The study demonstrates the efficacy of deep learning techniques in accurately identifying tumors within MRI images, potentially providing a more efficient and reliable diagnostic tool. Rammurthy et al. [38] explores a unique approach by integrating Whale Harris Hawks Optimization (WHHO) with deep learning classifiers for brain tumor detection using MRI images. The use of WHHO enhances the training process, optimizing the classifier's performance in identifying brain tumors from MRI scans. Raja et al. [39] a hybrid approach is proposed, combining deep autoencoders with Bayesian fuzzy clustering-based segmentation to classify brain tumors. This method demonstrates how advanced machine learning techniques can improve the precision of brain tumor classification by effectively segmenting the tumors within medical images. Haubolb et al. [40] research focuses on non-invasive tumor analysis, specifically for cerebral gliomas, using multiparametric 18F-FET PET-MRI and MR Fingerprinting. The study seeks to decode and phenotype tumors, providing valuable insights into their characteristics without the need for invasive procedures. This approach holds significant promise for advancing the diagnosis and treatment of brain tumors.

3. DUAL-WAY F^2M^3SLNN FRAMEWORK

The main target of the proposed methodology is to detect tumor from scan image. To improve image quality, the pre-processing is implemented that is huge supportive for further treatment. Here, both MRI and PET scan images are utilized for analyzing. Furthermore, features of MRI and PET images are fused which will integrate the merits of two modalities that are intentionally used for tumor diagnosis. Henceforth, in this paper multi-modality based tumor classification is proposed by proposing Dual-way F^2M^3 SLNN framework. Fig 1 represents the workflow of overall proposed Dual-way F^2M^3 SLNN framework. The proposed Dual-way F^2M^3 SLNN framework is defined as follows,

Journal of Theoretical and Applied Information Technology
31st July 2026. Vol.104. No.14

ISSN: 1992-8645 www.jatit.org E-ISSN: 1817-3195

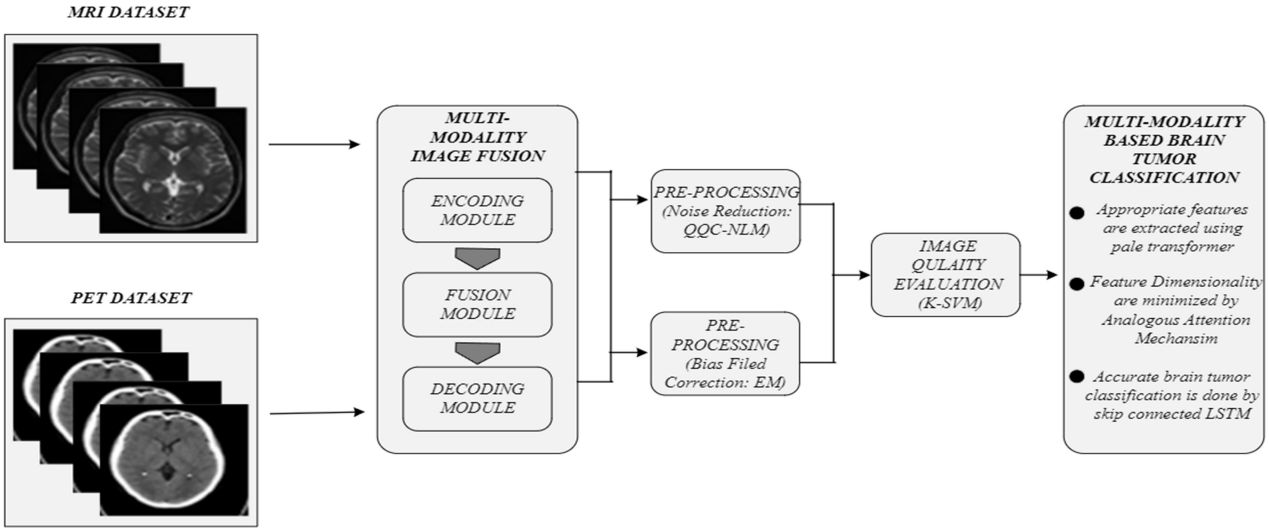

Fig.1 Overall Workflow of Proposed Dual-way F^2M^3 SLNN Framework

3.1. Multi-Modality Fusion

As the two diverse images such as MRI and PET are obtained from two diverse datasets by means of same position. Since, there will be general feature between two obtained images. Furthermore, the analysis two separate images also work with information loss and quality issues. For that, we have fused those obtained images using TangleNet module. The TangleNet module accepts input as I^{MRI} and I^{PET} respectively. The output of each input is represented as O^{MRI} and O^{PET}, then the fused output is represented as F. There are two sub-modules included in TangleNet module as encoding, fusion and decoding module respectively.

3.1.1 Encoding module

Input images are afford to the encoding sub-module where the images separate features are extracted individually. The extracted features from each images are flattened and symbolized in terms of temporal and spatial illustration respectively. To be more specific, the encoding module comprised of four dense layer with integration of convolution layer, rectilinear unit activation function and normalization layer (Conv+ReLu+BN).

3.1.2 Fusion Module

The feature map obtained from two input images via pale-structured transformer block is fed into fusion module. The fusion module utilize average norm technique (ANT) to fuse the both feature maps. Then, the feature maps fusion can be mathematically expressed as,

$$fm_f^n(r,s)=fm_{MRI}^n(r,s)+fm_{PET}^n(r,s) \quad (1)$$

Here, $fm_{MRI}^n(r,s)$ and $fm_{PET}^n(r,s)$ can be represented as feature maps of MRI and PET respectively. And then, $fm_f^n(r,s)$ is the feature map of fusion in which the number of feature maps are indicated as n. Overall, the two feature maps are fused by ANT as per their vividness in feature characteristics. ANT formulation is defined as,

$$fm_f^n(r,s)=\frac{1}{3}\left(fm_{MRI}^n(r,s)+fm_{PET}^n(r,s)\right) \quad (2)$$

From the formulation of aforementioned technique, the fused feature map weight is expressed as,

$$\varpi_f(r,s)=\|fm_f^n(r,s)\|_1 \quad (3)$$

Next, we can determine the activity level of feature maps can be formulated as,

$$\widehat{\varpi}_f(r,s)=\frac{\sum_{t=-q}^{q}\sum_{d=-q}^{q}\varpi_f(r,t,s+d)}{(2q+1)^2} \quad (4)$$

In above mentioned equation, the block is defined as q. At last, the overall fusion can be formulated in equation,

$$\widehat{\varpi}_f(r,s)=\square_f(r,s)\times fm_f^n(r,s)+\left(1-\square_f(r,s)\right) \quad (5)$$

Where $\square_f$ is denoted as fusion co-efficient that is defined as below,

$$\square_f(r,s)=\frac{\widehat{\varpi}_f(r,s)}{\widehat{\varpi}_f(r,s)+\varpi_f(r,s)} \quad (6)$$

3.1.3 Decoding Module

The fused feature is then afforded to the decoding module that executes image reconstruction. Specifically, the feature maps of fuse are passed to processed with four successive layers of convolutional and fully connected. The resultant outcome from decoding module is high appropriate fused brain image F_{img}. Finally, the proposed TangleNet loss function is generated by means of pixel loss. The mathematical formulation of loss function is defined as,

$$L=L_{MRI}+L_{PET}+\frac{1}{2}(L_{MRI+PET}) \quad (7)$$

From the above equation, L indicated as loss function. The parameters L_{MRI} and L_{PET} are the loss function of MRI and PET images respectively. $L_{MRI+PET}$ is the general image feature loss function.

3.2 Pre-Processing

In this investigation, we harnessed the power of MRI and PET fused images and employed pre-processing methods to enhance image quality. These techniques encompassed the removal of noise, the enhancement of biases, and the assessment of image quality:

3.2.1 Noise reduction

MRI and PET fused images frequently suffer from various types of noise, such as Speckle noise, Rician noise, Gaussian noise, and Salt and pepper noise. In our efforts to boost the quality of both MRI and PET fused images, we utilized Quaternion Quasi-Chebyshev with Non-Local Means (QQC-NLM). This algorithm use entire adapt of self-similarities of high degree insides the images to reduce the noise, so that similarity metric between image patches plays vital role in its noise reduction performance. For two patches of any images $\partial_i(a,b)$ and $\partial_j(a,b)$ along with $\alpha\times\alpha$, represents their untainted quaternion illustration as,

$$\beta_i(a,b)=\partial_i^G(a,b)\gamma \quad (8)$$

$$\beta_j(a,b)=\partial_j^G(a,b)\gamma \quad (9)$$

Where G denotes the single channels of grey color images. The QQC image patches distances ∂_i is expressed as,

$$cd=\left(\beta_i,\beta_j\right)=\max_{a,b}|\beta_i(a,b)-\beta_j(a,b)| \quad (10)$$

$$=\max_{a,b}\left\{\sqrt{\left[\partial_i^G(a,b)-\partial_j^G(a,b)\right]^2}\right\} \quad (11)$$

A QQC distance have noticeable advantages across quaternion Euclidean distance in default QQC-NLM: The QQC distance procedures the utmost distance in entire grey channels during the total distance is measures Euclidean distance, hence the image similarity measures by Quasi-Chebyshev distance collect the structural similarity unvarying for every channel of images. Moreover, bilateral filter generalize into as quaternion bilateral filter (QBF) and utilize QBF for pre-processing step in QQC-NLM where the QBF of untainted quaternion illustration $\{\varphi(m,n)\}_{m,n}$ of any grey image is described as,

$$\widehat{\varphi}(a,b)=\frac{\sum_{m,n}e^{-g^2[(a,b),(m,n)]/2\varrho_{g\times}^2}e^{-qg^2[\varphi(a,b),\varphi(m,n)]/2\varrho_r^2}\times\varphi(m,n)}{\sum_{m,n}e^{-g^2[(a,b),(m,n)]/2\varrho_{g\times}^2}e^{-qg^2[\varphi(a,b),\varphi(m,n)]/2\varrho_r^2}} \quad (12)$$

Here, qd[.] and g[.] denotes the quaternion Euclidean distance and Euclidean distance, respectively. For high level noise, our algorithm utilize QBF initially and then continued by QQC-NLM for image denoising. By this way, this filters excel at eliminating noise while preserving crucial edge features.

3.2.2 Bias enhancement

Correcting bias fields is a pivotal step in alleviating intensity irregularities arising from magnetic fields. This correction aids in clarifying distinctions among brain tissues, primarily with the goal of reducing classification errors. The non-uniformity in magnetic field intensity causes variation in intensity values among voxels within the same tissue. This variation exhibits a gradual shift in intensity according to an unidentified model. Consequently, it becomes essential to estimate this model to correct the intensity values. In our research, we initiate the process by assigning labels to voxels to estimate the bias field, which is then used for intensity correction.

To achieve this, we perform an initial coarse segmentation of the image utilizing an EM algorithm, executed in segments across the entire volume. Subsequently, by amalgamating partial labeling outcomes with the final labels assigned to image voxels, we estimate the bias field as a hyper-surface represented by δ. Here, δ(u,v,w)signifies the ratio between the mean intensity around the voxel δ(u,v,w) and the mean intensity at a reference voxel (uτ,vτ,wτ) belonging to the same tissue type and having the highest membership certainty among all the voxels within the current sub-volume.To calculate the mean intensity value, we consider a

neighborhood consisting of a 3x3 voxel grid centered around a given voxel.

$$\delta(u,v,w)=\frac{\hat{I}(u,v,w)}{I(u^{\tau},v^{\tau},w^{\tau})} \quad (13)$$

Here,

$$\hat{I}(u,v,w)=\frac{1}{|\chi(u,v,w)|}\sum_{i\epsilon\chi(u_i,v_i,w_i)} I(u^{\tau},v^{\tau},w^{\tau}) \quad (14)$$

Where $\chi(u,v,w)$ indicates the voxels neighboring set $\{(u_i,v_i,w_i)\}$ of (u,v,w) which depends to similar tissue.

We retained a voxel, denoted as i, for bias estimation only if its associated membership certainty, represented by the probability $\rho^{T}i$, exceeded a predefined threshold, T_{ρ}. For the remaining voxels, we computed the bias field through interpolation, employing a Lagrangian hyper-surface that we introduce in this study. Moreover, to create this hyper-surface, we selected a set of voxels sampled from those for which the bias field had already been estimated. For each group of connected unlabeled voxels where bias field computation was necessary, we defined an enclosing volume area. Within this volume, we carefully selected a set Ω of voxels distributed approximately uniformly. These selected voxels served as control points for generating the Lagrangian hyper-surface, enabling us to estimate the bias field within this specific area. Lagrangian interposed hyper-surface $\hat{\delta}(u,v,w)$ which includes volume area that mathematically defined as,

$$\hat{\delta}(u,v,w)=\sum_{\kappa\epsilon\Omega}\delta_{\kappa}\frac{\prod_{i\neq\kappa}(u-u_i)(v-v_i)(w-w_i)}{\prod_{i\neq\kappa}(u_{\kappa}-u_i)(v_{\kappa}-v_i)(w_{\kappa}-w_i)} \quad (15)$$

Here, $\{(u_{\kappa}, v_{\kappa}, w_{\kappa})\epsilon\Omega\}$ denotes the control points set which comprising volume area utilized to define Lagrangian polynomial. Moreover, a specific point $(u_{\kappa}, v_{\kappa}, w_{\kappa})$ is selected as a control point under two conditions: firstly, it must have been labeled as belonging to a particular tissue, and secondly, its membership certainty exceeds the threshold T_{ρ}. After the computation of the bias field across the entire MRI and PET fused image volume, the correction of voxel intensity $I^{e}(u,v,w)$ at each voxel (u,v,w) within the volume is carried out as follows:

$$I^{e}(u,v,w)=I(u,v,w)\times\hat{\delta}(u,v,w) \quad (16)$$

The acquired corrected image I^{e} is contemplated as bias field-free which can be utilized for further processing.

3.2.3 Image quality evaluation

To validate the quality of the pre-processed MRI and PET fused image, we employed a Kernel Support Vector Machine (K-SVM) for the assessment of image quality. If the image quality met predefined threshold criteria, we considered it suitable for subsequent analysis, signifying the effectiveness of noise reduction and enhancement. If not, we iterated on the aforementioned pre-processing steps to achieve improved image quality.

A Kernel work is differentiated as potential that correlated to point result of vector of two component in few expanded space as,

$$K(u,v)=\psi(u)'\psi(v)' \quad (17)$$

This extension in SVM is inspired with surface of non-linear decision which can classify non-linear individual data. The kernel is the non-stationary kernel which consists of degree (d), coeff (c) and gamma (g) are parameters. The polynomial kernel is significant for evaluation where overall pre-processed fused image is normalized. For polynomial degree d, then this kernel is expressed as,

$$K(u,v)=(g^{*}u^{*}v+c)^{d} \quad (18)$$

Where u and v are denoted as vector of input space which is that the feature vector are estimated from training and testing instances and $c^{3}0$ refers to the free parameter transaction off the impact of higher-order opposed to low-order conditions of polynomial. Basically, this function is distinctive case of logistic sigmoid function which is defined as,

$$S(t)=\frac{1}{1+e^{-t}} \quad (19)$$

After eliminating the noise from the input image, it undergoes an additional step for quality evaluation. This quality assessment process aims to measure the image's overall quality. To be more precise, the quality assessment module examines whether the image meets the required quality standards for further processing. In this quality assessment, the proposed approach employs a threshold-based method. A predefined threshold value, denoted as λ, is established for all the pre-processed images. The quality assessment formulation is presented as follows,

$$\begin{cases} \text{If } F_{img}\geq\lambda, & \text{Allowed} \\ \text{If } F_{img}<\lambda, & \text{Not-allowed} \end{cases} \quad (20)$$

In accordance with the equation above, when the quality of the pre-processed image exceeds or

equals λ, it proceeds to the classification module. Otherwise, it continues to undergo pre-processing until it attains a higher image quality

3.3. *Multi-modality Based Brain Tumor Classification*

Following the preprocessing of MRI and PET fused images, both data streams are input into the Dual-Way F2M3SLNN model. This model incorporates a pale transformer, a multi-scale attention mechanism, and a skip-connected LSTM in a dual configuration. Initially, relevant features are extracted using the pale transformer and then pass through a fusion network based on the skip-connected LSTM algorithm. Within this fusion network, a novel composite attention learning mechanism, complemented by a three-level fusion strategy, is employed to comprehensively integrate the features from both data sources.

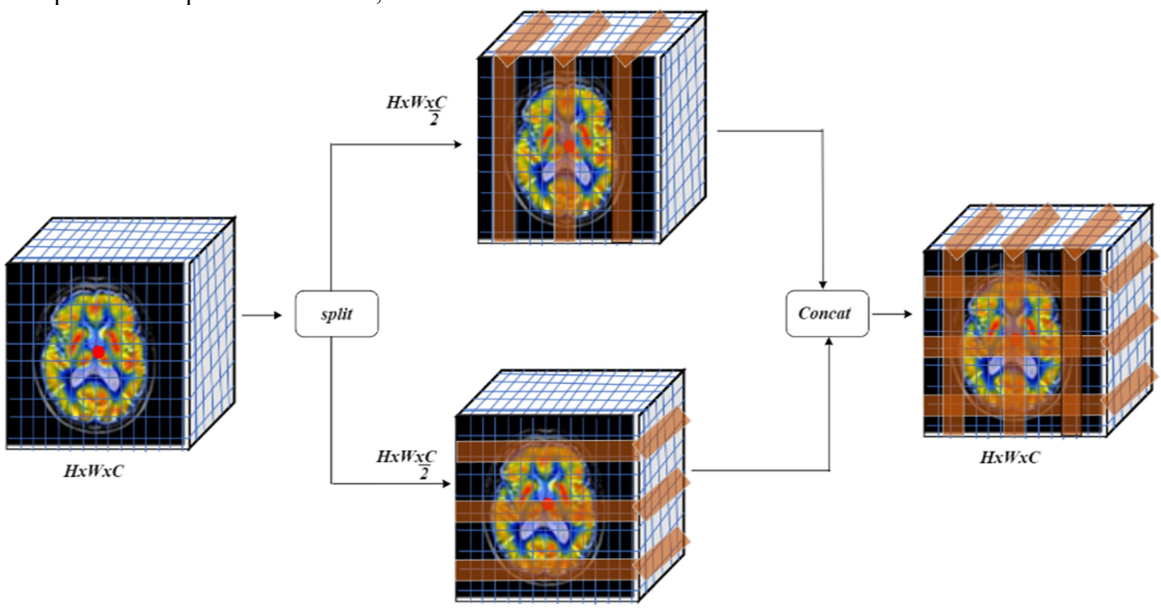

Fig.2 Pictorial Representation of PS-SA

3.3.1 Dual-Way feature extraction via pale transformer module

Here, we initially described pale-structured self-attention (PS-SA) and its effectual parallel illustration. After that, the Pale transformer block arrangement is provided. At last, we define overall architecture and alternates configuration of backbone of pale transformer.

(a) Pale-Structured Self-Attention

For collecting dependencies speckled from short-range to long-range, we utilized PS-SA as shown in fig.2, which determines self-attention along within pale-structured region. Single pale comprises $\mathcal{S}_x$ interweaved rows and $\mathcal{S}_c$ interweaved columns, that refuges region comprising $(\mathcal{S}_x W+\mathcal{S}_c H-\mathcal{S}_x \mathcal{S}_c)$ tokens. We describe $(\mathcal{S}_x,\mathcal{S}_c)$ as size of pale. Provided an input feature map $X \square R^{H\times W\times c}$, we initially divide it into several pales $\{P_1,\ldots,P_N\}$ with dissimilar size $(\mathcal{S}_x,\mathcal{S}_c)$, where $P_i \epsilon R^{(\mathcal{S}_x W+\mathcal{S}_c H-\mathcal{S}_x \mathcal{S}_c)\times c}$, $i \epsilon \{1,2,\ldots,N\}$.The number of pales is alike to $N=\frac{H}{\mathcal{S}_x}=\frac{W}{\mathcal{S}_c}$, that can be assured through padding function. For entire pales, intervals among adjacent or columns are similar and then self-attention is accomplished within every pales separately. Moreover, the PS-SA amenable filed attention is appropriately richer and wider than other default self-attention scheme.

(b) Effectual Parallel Illustration

To further enhance the effectual, we crumble vanilla PS-SA which is above mentioned into the attention of row-wise and column-wise token sets, respectively. To be more specific, we initially spilt input feature $X \square R^{H\times W\times c}$ into two autonomous parts $X_x \square R^{H\times W\times \mathcal{S}}$ and $X_c \square R^{H\times W\times \frac{c}{2}}$ at channel dimension, that are divided into several sets for attention of row-wise and column-wise respectively.

$$X_x=[X_x^1,\ldots,X_x^{N_x}],\ X_c=[X_c^1,\ldots,X_c^{N_c}] \qquad (21)$$

Where $N_x=H/\mathfrak{S}_x$, $N_c=W/\mathfrak{S}_c$, $X_x^i \varepsilon R^{\mathfrak{S}_x \times W \times c}$ comprise $\mathfrak{S}_x$ interweaved rows, and $X_c^i \varepsilon R^{H \times \mathfrak{S}_c \times c}$ comprise $\mathfrak{S}_c$ interweaved columns. After that, self-attention is performed within every token sets of row-wise and column-wise, respectively. We utilize three individual convolution layers ϕ_Q,ϕ_K and ϕ_V to compute the query, key and value.

$$Y_x^i=MSA\left(\phi_Q(X_x^i),\phi_K(X_x^i),\phi_V(X_x^i)\right) \quad (22)$$

$$Y_c^i=MSA\left(\phi_Q(X_c^i),\phi_K(X_c^i),\phi_V(X_c^i)\right) \quad (23)$$

Where i□ {1,2,…,N}, and MSA signifies the multi-head self-attention. At last, the attention of row-wise and column-wise outputs are concatenated with dimension of channel, outcoming of final output Y□ $R^{H \times W \times c}$,

$$Y=Concat(Y_x,Y_c) \quad (24)$$

Where $Y_x=\left[Y_x^1,\ldots,Y_x^{N_x}\right]$ and $Y_c=\left[Y_c^1,\ldots,Y_c^{N_c}\right]$. Besides, the padding function only requires to assure H is divisible via $\mathfrak{S}_x$ and W is divisible via $\mathfrak{S}_c$ relatively than $\frac{H}{\mathfrak{S}_x}=W/\mathfrak{S}_c$. Henceforth, it is also conductive to evading extreme padding.

(c) Pale Structure Transformer Module

This block comprise of three consecutive parts, the provisional position coding (PPE) for vigorously determining the position embedding, the proposed PS-SA block for extract the features by contextual information, and the MLP block of feature projection. The l-th block forward pass can be mathematically formulated as follows:

$$\hat{\chi}^l=\chi^{l-1}+PPE(\chi^{l-1}) \quad (25)$$

$$\hat{\chi}^l=\hat{\chi}^l+PS\text{-}SA\left(LN(\hat{\chi}^l)\right) \quad (26)$$

$$\chi^l=\hat{\chi}^l+MLP\left(LN(\hat{\chi}^l)\right) \quad (27)$$

Where LN(.) denotes to layer normalization. Here, the PPE is accomplished as general convolution of depth-wise, that is widely utilized. Furthermore, PS-SA block described in eq (7) is generated by consecutively executing eq (1) to eq (3). MLP block described in eq (8) comprise of layers of two linear projection extend and convention the consecutively embedding dimension.

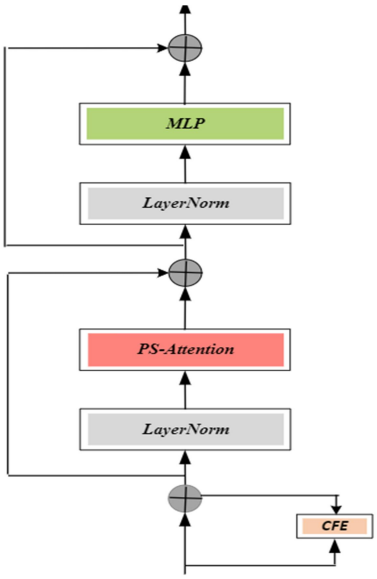

Fig.3 Pale Transformer Module

3.3.2 Analogous attention mechanism

The pale-structured transformer layer produces accurate feature maps denoted as fm_f^n feeds them into analogous attention layers. Within these layers, the MRI and PET fused images undergo channel and spatial attentions separately. These channel and spatial attention layers operate concurrently. Subsequently, fm_f^n is passed to the spatial attention layer, comprising three depth-wise 2D convolutional layers and ReLU activation layers. The mathematical formulation for the spatial attention layers can be expressed as follows,

$$fm_f^{nSA}=\vartheta^2\left(\left(\varepsilon^2\left(\vartheta^2\left(\varepsilon^1\left(\vartheta^2(fm_f^n)\right)\right)\right)\right)\right) \quad (28)$$

From the aforementioned equation, the feature maps are represented as fm_f^n, then the depth wise 2D conc layers and activation function can be signified as ϑ^2 and ε^2 respectively and the outcome of spatial attention layer is fm_f^{nSA}. Likewise, the channel attention layer encompass of single activation layer and 2 depth wise convolution layers respectively which can be mathematically defined as,

$$fm_f^{nCA}=\vartheta^2\left(\varepsilon^1\left(\vartheta^1(fm_f^n)\right)\right) \quad (29)$$

3.3.3. LSTM with skip connected based tumor classification

In classifier consists of skip connection with LSTM where the skip connection layer integrates the fused features are collected from fusion module

and the tumor classified utilizing LSTM layer into single vector the method of concatenation skip connection. The addition of skip connection skips the layer of convolution and add the input fused feature directly to output that permits the input data to pass to output. The ϱ represents input data, F(ϱ) denotes the output obtained from Layer 2, and F(ϱ)+ϱ signifies the outcome generated using the addition skip connection approach, which combines the input data with the Layer 2 output. In contrast to the addition skip connection, the concatenation skip connection involves merging the input data vector with the output vector from Layer 1. This facilitates the retention of the maximum amount of information within each layer of the deep learning model, consequently enhancing model accuracy. This study employed the concatenation skip connection method.

LSTMs employ a gating mechanism, involving element-wise multiplication of the input, to regulate the flow of information. The LSTM cell state undergoes updates based on the activation of these gates. Input data passed into an LSTM is processed through distinct gates, namely, the input gate, output gate, and forget gate, each responsible for specific operations on the cell memory. In this context, C_{t-1} denotes the previous cell state, h_{t-1} signifies the previous hidden state, X_t corresponds to the input data for the LSTM, C_{t-1} represents the updated cell state, h_{t-1} signifies the updated hidden state, and □ and □ denote vector operations. Additionally, □ symbolizes the sigmoid function, which can be expressed as follows:

$$\text{sigmoid}(X)=\frac{1}{1+e^{-}} \quad (30)$$

In this context, X represents the input data, and e denotes the natural constant. Finally, the term tanh corresponds to the hyperbolic tangent, which can be mathematically expressed as follows:

$$\tanh(X)=\frac{e^{X}-e^{X}}{e^{X}+e^{X}} \quad (31)$$

The forget gate in LSTM calculates the current information and considers the value of the previous hidden layer to decide how much of the past information to discard. The operation of the forget gate at time t can be represented using the following equation:

$$F_t=\sigma\left(w_{I_F}\left[h_{t-1},X_t\right]+b_F\right) \quad (32)$$

From the above equation, X_t denotes input vector, h_{t-1} is previous hidden layer vector. The parameters w_{I_F}, b_F and F_t is the weight, bias value and forget value. The output generated by the forget gate serves as input for the input gate, which assesses the significance of the current data and then stores it in a cell. The components of the input gate can be mathematically described using the following equation:

$$i_t=\sigma\left(\sigma\left(w_{I_F}\left[h_{t-1},X_t\right]+b_t\right)\right) \quad (33)$$

Furthermore, you can express the functions performed by the input gate layer and the tanh layer in the following manner:

$$\widehat{C}_t=\tanh\left(w_{I_C}\left[h_{t-1},X_t\right]+b_C\right) \quad (34)$$

The output gate derives a new cell state C_t using the following expression from the input gate:

$$C_t=F_t\times C_{t-1}+i_t\times\widehat{C}_t \quad (35)$$

Finally, the new hidden state h_t is determined by the output gate using the following equation:

$$□_t=\sigma_t\left(w_{I_□}\left[h_{t-1},X_t\right]+b_t\right) \quad (36)$$

$$h_t=\sigma_t\times\tanh(C_t) \quad (37)$$

Ultimately, drawing inspiration from transfer learning, a novel stepwise training strategy is devised to produce the final tumor classification result.

4. EXPERIMENTAL RESULTS

In this section, the result and discussion regarding brain tumor classification via pre-processing. We have conducted our proposed framework on MATLAB 7.12 version for execution which also enhance Dual-way F^2M^3 SLNN recommended technique. The recommended technique is performed in windows machine taking a processor of Intel Core i5 along with 1.6 GHz speed and RAM of 4GB. Furthermore, this technique has been detected on brain image gathered from MRI and PET datasets that are publicly accessible on internet. The input images are obtained from diverse resource (Brain Image Resources, internet) recommended technique in this paper. Besides, the performance is evaluated via equating and comparing the results with existing approaches.

4.1 *Evaluation Metrics*

System performance is verified by employing the valuation metrics such as accuracy, specificity, sensitivity, PPR, FPR, FNR and NPR that are illustrated below,

(a) Accuracy: Accuracy is estimated by measuring sensitivity and specificity which is denote as,

$$Acc=\frac{TP+TN}{TP+TN+FP+FN}\times 100 \quad (39)$$

(b) Specificity: Specificity is the multiple true negative ratio to the true negative and false positive ratio.

$$Specificity=\frac{\text{Number of TN}}{\text{Number of TN and Number of FP}}\times 100 \quad (40)$$

(c) Sensitivity: Sensitivity is the few true positives ratio to sum of the false negative and true positive as,

$$Sensitivity=\frac{\text{Number of TP}}{\text{Number of TP and Number of FN}}\times 100 \quad (41)$$

(d) Positive Predicted Rate (PPR): The fraction of positive experimentation significances that are contemplated as PPR which is formulated as,

$$PPR=\frac{TP}{FP+TP} \quad (42)$$

(e) False Positive Rate (FNR): FNR is evaluated as the number of inappropriate negative classification and divided through the total negative number. Moreover, it can also be evaluated as 1-specificity.

$$FPR=\frac{FP}{TN+FP} \quad (43)$$

(f) False Negative Rate (FNR): Number of inappropriate negative classifications to the total negative numbers is estimated as,

$$FPR=\frac{FN}{TP+FN} \quad (44)$$

(g) Negative Predictive Rate (NPR): Fraction of negative experimentation results that is considered as NPR,

$$NPR=\frac{TN}{FN+TN} \quad (45)$$

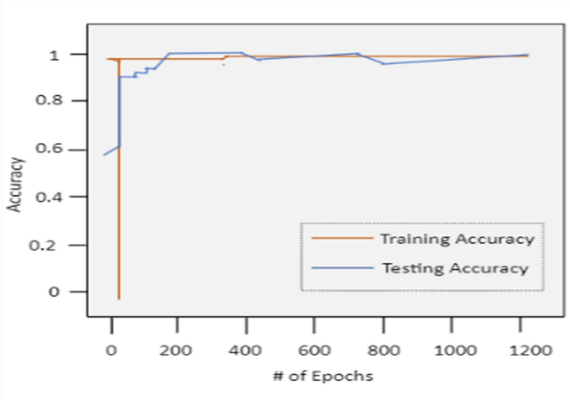

Fig .4 Training and Testing Accuracy Evaluation of Dual-way F^2M^3 SLNN Framework

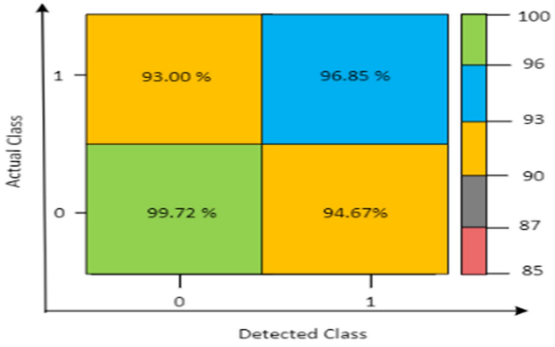

Fig.5 Confusion Matrix of Dual-way F^2M^3 SLNN

AUC-ROC curve represents the incorporated classification performance of proposed classifier on overall possible threshold. Achieving better AUC will enhancing the performance of classifier. Training and testing accuracy of proposed Dual-way F^2M^3 SLNN framework is defined in fig 4. Moreover, fig 5 illustrates the Dual-way F^2M^3 SLNN work performance and confusion matrix. Our methodology achieved the highest scores in metrics including sensitivity, specificity, accuracy, F1-score, PPR, and NPR, with values of 1.00, 0.98, 0.96, 0.97, 0.98, and 1.00, respectively, outperforming other previous techniques. Similarly, our method yielded the lowest values for FPR, FNR, and FDR, indicating superior performance compared to other methods. Refer to Figure 7 for a corresponding plot of the results of accuracy, sensitivity, specificity, F1-score and AUC.

4.2 Evaluation Results

Our proposed methodology is centered on the detection of brain tumors in MRI and PET images. To assess the performance of our pre-processing and classification approach, we conducted a comparative evaluation against state-of-the-art pre-processing and classification algorithms, considering metrics such as accuracy, sensitivity, and specificity. The experimental results unequivocally demonstrate the effectiveness of our approach in addressing a wide range of segmentation challenges by enhancing both the quality and accuracy of pre-processing while minimizing execution time.

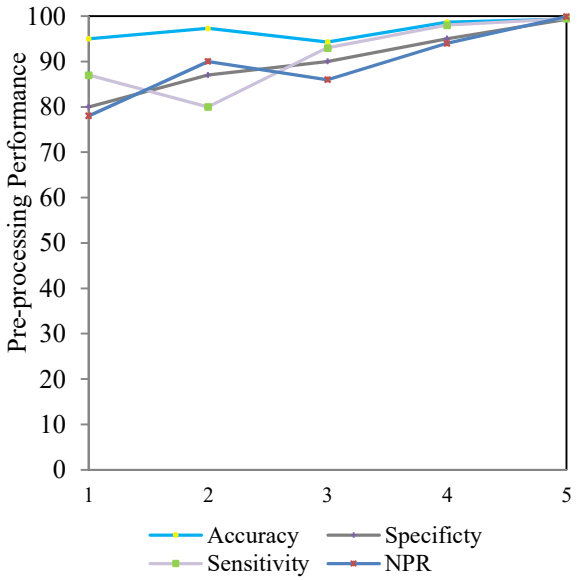

Fig.8 Performance Analysis of Pre-processing

The figure displayed above present a comparative analysis of pre-processing results. These comparisons aim to validate the effectiveness of our proposed multiple pre-processing methods when contrasted with existing pre-processing approaches. In Fig. 8, we assess the performance of the proposed methodology in terms of sensitivity. The proposed method achieves a maximum sensitivity of 95%, surpassing the 91.5% sensitivity achieved by performing noise reduction, bias filed correction using QQC-NLM and EM respectively. Besides, the image quality evaluation is executed by K-SVM where the image is accepted only if the pre-processing have performed effectively which are tends to enhance pre-processing accuracy. In that, we analyze the specificity performance of our proposed methodology. Here, our method achieves a remarkable maximum specificity of 99.5%, which significantly outperforms existing approaches. At last, Fig. 8 and Table I presents an analysis of accuracy, specificity and sensitivity where our proposed pre-processing method achieves maximum performance scores of 99.34%, 99.29%, and 99.45%, for images 1 to 5, respectively. Additionally, in Fig. 8, we observe a maximum NPR of 99.87%. Furthermore, in Figs. 8, our proposed methodology consistently outperforms existing image quality assessment approaches, as demonstrated by the results presented.

4.3. Comparison Analysis

In this section, we have conducted a comparative analysis between our proposed Dual-way F^2M^3 SLNN model and existing research. Specifically, we have considered two prior works. The primary objective of this study is to achieve accurate brain tumor classification through effective pre-processing. Our proposed approach has demonstrated superior performance across various metrics, including accuracy, specificity, sensitivity, F-measure, and ROC curve analysis. The subsequent subsection delves into the details of our experimental results, which were obtained through an extensive series of experiments involving several state-of-the-art machine learning models.

4.3.1 Performance analysis of fusion approaches

The following performance metrics such as structural similarity index metric (SSIM), entropy, mutual information (MI), peak signal to noise ratio (PSNR) and standard deviation (SI) metrics. In this sub-section, the performance of multi-modality fusion approaches are evaluated and compared with our proposed Dual-way F^2M^3 SLNN framework. Here, by means of several performance metrics accuracy, sensitivity, specificity, PPR, FPR, FNR and NPR. ODNN [21], Neuro-on [22], HFCMK [23], VAE [24] and EDF [25] approaches are compared with proposed feature fusion Dual-way F^2M^3 SLNN framework. Fig.9 illustrates the fusion performance of existing and proposed model. Additionally, the proposed method resulted in superior quality enhancement image and bias field corrected image with an effective brain tumor classification as compared with other fusion models. Further, Table illustrate objective comparison of existing approaches with proposed framework. At last, for overall performance metrics the proposed framework outstripped conformist approaches by means of quantitative performance.

Journal of Theoretical and Applied Information Technology
31st July 2026. Vol.104. No.14

ISSN: 1992-8645 www.jatit.org E-ISSN: 1817-3195

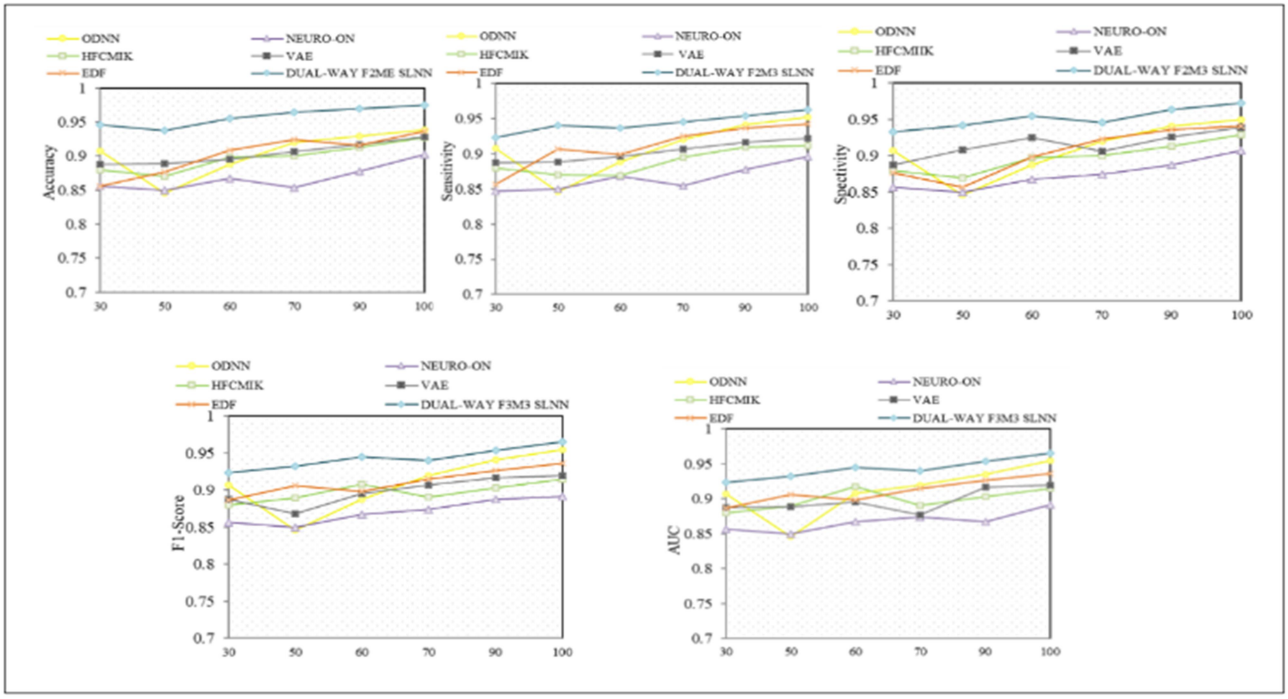

Fig.7 Evaluation Results of Accuracy, Sensitivity, Specificity, F1-score and AUC

Table 1. Pre-processing Analysis

Models	Fused Image	Pre-processed Image
ODNN	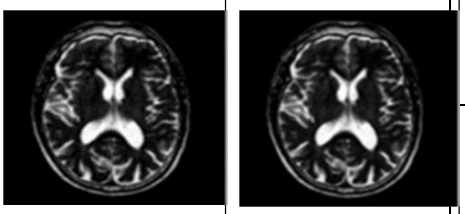	
Neuro-on	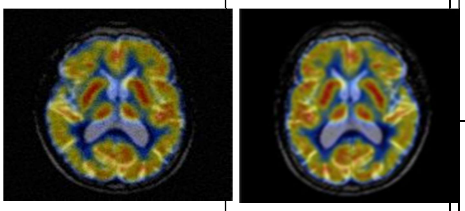	
HFCMIK	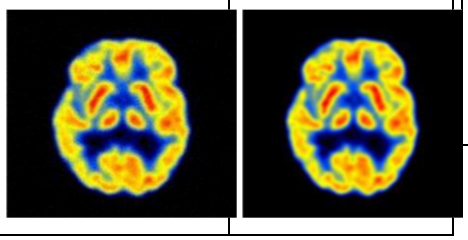	
VAE	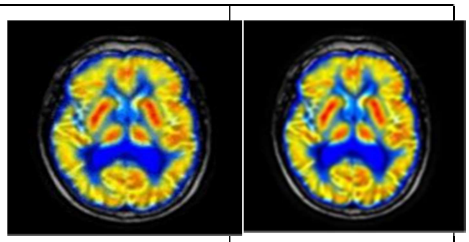	
EDF	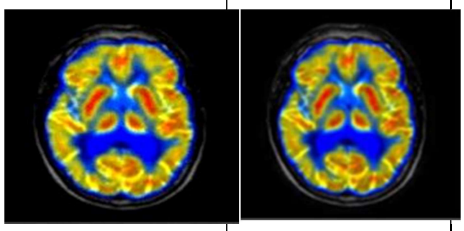	
Dual-way F^2M^3 SLNN	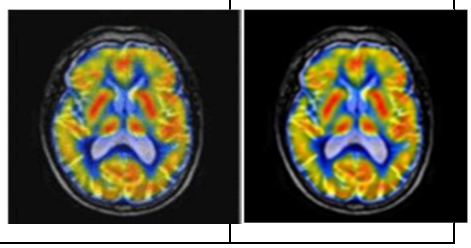	

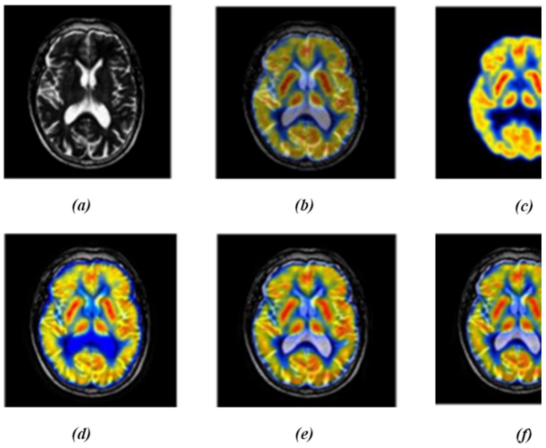

Fig.9 MRI-PET Resultants (a) ODNN, (b) Neuro-on, (c) HFCMK, (d) VAE, (e) EDF & (f) Dual-way F^2M^3 SLNN

Table 2 MRI-PET Image Fusion Approaches Performance Analysis

Metrics	ODNN	Neuro-on	HFCMK	VAE	EDF	Dual-way F^2M^3 SLNN
SSIM	0.712	0.723	0.762	0.845	0.927	0.978
Entropy	7.452	8.750	9.648	10.760	11.978	14.890
MI	0.674	0.778	0.808	1.567	1.767	1.994
PSNR	29.568	37.594	43.382	45.558	47.734	52.482
SI	0.256	0.221	0.167	0.092	0.085	0.057

Fig 10 Compares the proposed Dual-way F^2M^3 SLNN framework's MRI-PET image fusion outcome with visual performance of existing approaches such as ODNN [21], Neuro-on [22], HFCMK [23], VAE [24] and EDF [25]. Besides, the recommended technique generated greater brightness and contrast, along with effective tumor highlight while comparison to methods from traditional methods utilized already. Table VI presents an objective comparison of our approach with other established methods. Notably, our strategy consistently outperforms traditional methods across all performance parameters, as visually depicted in Figure 10.

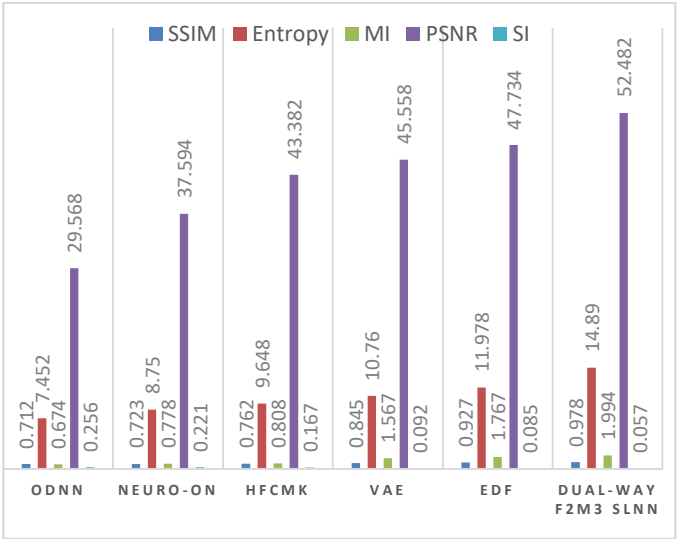

Fig 10 Graphical Representation of Image Fusion Comparison of Existing Approaches with Proposed Work

4.3.2 Performance analysis of classification approaches

This section offers an in-depth simulation analysis of our proposed DLPNN classification approach in comparison to traditional methods. The study evaluates the performance of these methods using a variety of metrics, including diagnosis accuracy (DACC), diagnosis sensitivity (DSEN), diagnosis specificity (DPEC), diagnosis precision (DPR), diagnosis negative predictive rate (DNPR), diagnosis false positive rate (DFPR), diagnosis false discovery rate (DFDR), diagnosis false negative rate (DFNR), diagnosis F1-score (DF1), and diagnosis Matthew's correlation coefficient (DMCC).

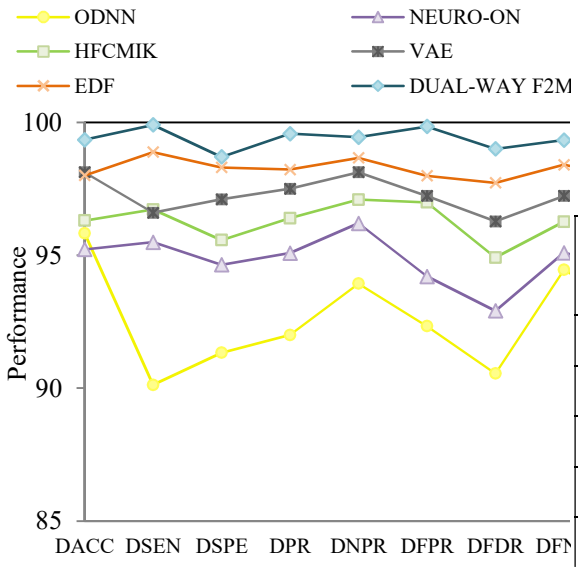

Fig.11 Classifier Performance Analysis of Fusion Approaches

4.4. Comparison Analysis of Classifier in Fusion Models:

Here, at first the performance analysis of classifier in fusion models are evaluated and compared. Table VIII represents the classification performance of the proposed Dual-way F^2M^3 SLNN approach with existing works PPR, FPR, FNR and NPR. ODNN [21], Neuro-on [22], HFCMK [23], VAE [24] and EDF [25]. Table VIII also illustrates that proposed methodology outperformed while comparing to other existing methods which is further proven in graphical representation of fig 13. The table above presents the classification results obtained using our proposed Dual-way F^2M^3 SLNN framework in comparison to the conventional approaches. Our methodology achieved the highest scores in performance metrics of classifiers mentioned above which outperforming other previous classifiers. The main reason for attaining such high performance of classifiers is due to performing accurate fusion, pre-processing and classification. By utilizing TangleNet, we have fused both MRI and PET images based on extracting appropriate features. After that, we have pre-processing the fused images in terms of noise reduction and bias filed correction using QQ-NLM and EM. Besides, for analysing the quality of pre-processed image, the image quality evaluation process is performed by K-SVM. Finally, for brain tumor diagnosis the significant features are extracted from pre-processed fused image and then attention mechanism is adapted for minimizing the feature dimension thereby minimizing model complexity. At last, the skip connection based LSTM is utilized for accurate brain tumor diagnosis.

Table 3. MRI-PET Image Fusion Approaches Classifiers Performance Analysis

Metrics	ODNN	Neuro-on	HFCMIK	VAE	EDF	Dual-way F^2M^3 SLNN
DACC	95.83	95.22	96.3	98.12	98	99.34
DSEN	90.12	95.49	96.72	96.6	98.88	99.90
DSPE	91.33	94.64	95.57	97.10	98.3	98.7
DPR	92	95.08	96.39	97.5	98.22	99.57
DNPR	93.93	96.2	97.09	98.12	98.66	99.44
DFPR	92.33	94.20	96.99	97.23	97.99	99.84
DFDR	90.55	92.91	94.91	96.27	97.72	99
DFNR	94.45	95.09	96.26	97.23	98.40	99.33
DF1	93.11	94.46	95.28	96	97.85	99.4
DMCC	91.74	93.75	96.28	97.23	98.81	99.32

4.5. Comparison Analysis of Classifier in Non-Fusion Models:

In this initial step, we commence by assessing and contrasting the performance analysis of the classifier within fusion models. Table 4 showcases the classification performance of our novel Dual-way F^2M^3 SLNN approach, juxtaposed against existing methods such as PPR, FPR, FNR, and NPR, as well as reference models like BTFS-Net [27], Dark-Net [28], YOLO-CNN [34] based on MRI images, CNN [36] and DAE [39] based on PET images respectively. The data in Table VIII unequivocally demonstrates the superior performance of our proposed methodology when compared to the aforementioned existing methods, a fact that is further substantiated through graphical representation in Figure 13. Thus, the table above presents a comprehensive overview of the classification results achieved through our innovative Dual-way F^2M^3 SLNN framework in relation to conventional approaches. From the graphical representation and table evaluation, it is clearly visible that fusion models achieves betterment performance while compare with non-fusion models. Specifically, from that our proposed work achieves superior performance. The reason for achieving such low performance is that, in non-

fusion works can obtain the information from either MRI or PET images. Furthermore, lack of image fusing and pre-processing are leads to attaining low performance.

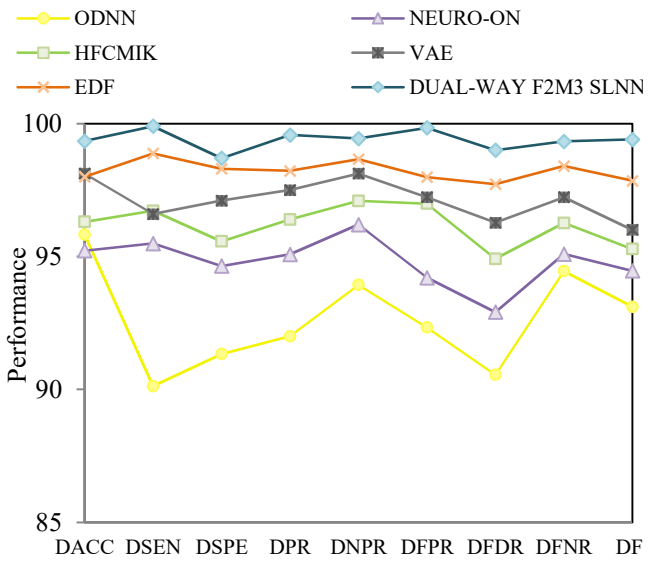

Fig.12 Classifier Performance Analysis of Non-Fusion Approaches

Table 4 MRI-PET Image Non-Fusion Classifiers Approaches Performance Analysis

Metrics	ODNN	Neuro -on	HFCMIK	VAE	EDF	Dual-way F^2M^3 SLNN
DACC	85.83	84.22	86.3	90.12	91	99..34
DSEN	80.12	85.49	86.72	86.6	91.88	99.90
DSPE	81.33	84.64	85.57	87.10	88.3	98.7
DPR	82	85.08	86.39	90.5	92.22	99.57
DNPR	83.93	86.2	87.09	92.12	91.66	99.44
DFPR	82.33	84.20	86.99	87.23	92.99	99.84
DFDR	83.55	82.91	84.91	86.27	87.72	99
DFNR	84.45	85.09	86.26	87.23	92.40	99.33
DF1	83.11	84.46	85.28	89	91.85	99.4
DMCC	81.74	83.75	86.28	87.23	88.81	99.32

5.CONCLUSION

In conclusion, brain tumors, characterized by the uncontrolled proliferation of cells, demand precise localization and size identification within the medical diagnostic realm. Magnetic Resonance Imaging (MRI) and Positron Emission Tomography (PET) serve as indispensable tools in this pursuit, albeit with the challenge of low boundary pixel sensitivity. Recent attempts to address this challenge have introduced an efficient fusion-based approach, yet these approaches have shown limitations in delivering accurate results. To overcome these limitations, our study introduces the Multi-modality-based brain tumor classification method known as the Dual-way F^2M^3 SLNN framework. We start by fusing MRI and PET information using TangleNet via the Average Norm Technique (ANT). This fusion is further improved through noise reduction and bias field correction using Quaternion Quasi-Chebyshev with Non-Local Means (QQC-NLM) and Expectation Maximization.

We ensure the quality of the pre-processed images through evaluation using Kernel Support Vector Machine (K-SVM). Subsequently, we extract relevant features using the Pale structure transformer and reduce feature dimensionality through the Analogous Attention Mechanism. Finally, we achieve accurate brain tumor classification through the application of Skip-connected Long Short-Term Memory (SC-LSTM). Our proposed Dual-way F^2M^3 SLNN framework, implemented in MATLAB, significantly enhances model performance. Evaluation using various performance metrics, including accuracy, sensitivity, specificity, F1-Score, and AUC, consistently demonstrates the superior performance of our framework compared to existing methods. This innovative approach holds promise for improving the accuracy and reliability of brain tumor detection and classification in medical imaging.

REFERENCES

[1]. Loizou, L., Demetriou, A., Erdmann, F., Borkhardt, A., Brozou, T., Sharp, L., & Mcnally, R. (2022). Patterns and temporal trends in the incidence of childhood and adolescence cancer in Cyprus 1998-2017: A population-based study from the Cyprus Paediatric Oncology Registry. *Cancer epidemiology, 80*, 102239 .

[2]. Davies, O., & Taylor, A.J. (2020). Refining the "double two-thirds" rule: Genotype-based breed grouping and clinical presentation help predict the diagnosis of canine splenic mass

lesions in 288 dogs. *Veterinary and comparative oncology*.

[3]. Ghiaseddin, A.P., Shin, D.H., Melnick, K.F., & Tran, D.D. (2020). Tumor Treating Fields in the Management of Patients with Malignant Gliomas. *Current Treatment Options in Oncology, 21*.

[4]. Snow, A., Struycken, L., Koç, M., Greco, J.M., Zhu, Y., In, G.K., Dorff, T., & Lang, J.D. (2019). Abstract P3-12-14: Incidence of radiation induced sarcoma attributable to radiotherapy in adults: A population-based study of the SEER cancer registry across 17 primary tumor sites. *Poster Session Abstracts*.

[5]. Uwishema, O., Frederiksen, K.S., Badri, R., Pradhan, A.U., Shariff, S., Adanur, I., Dost, B., Esene, I.N., & Rosseau, G.L. (2023). Epidemiology and etiology of brain cancer in Africa: A systematic review. *Brain and Behavior, 13*.

[6]. Fitzpatrick, S.M., Brogan, D.M., & Grover, P. (2022). Hand Transplants, Daily Functioning, and the Human Capacity for Limb Regeneration. *Frontiers in Cell and Developmental Biology, 10*.

[7]. Raja, P.M., & rani, A.V. (2020). Brain tumor classification using a hybrid deep autoencoder with Bayesian fuzzy clustering-based segmentation approach. *Biocybernetics and Biomedical Engineering, 40*, 440-453.

[8]. Kuraparthi, S., Kollati, M., Valiveti, H.B., & Karuna, G. (2022). Segmentation and detection of brain tumor through optimal selection of integrated features using transfer learning. *Multimedia Tools and Applications, 81*, 27363 - 27395.

[9]. Magadza, T., & Viriri, S. (2021). Deep Learning for Brain Tumor Segmentation: A Survey of State-of-the-Art. *Journal of Imaging, 7*.

[10]. Deepak, S., & Ameer, P.M. (2020). Automated Categorization of Brain Tumor from MRI Using CNN features and SVM. *Journal of Ambient Intelligence and Humanized Computing, 12*, 8357 - 8369.

[11]. Chanu, M.M., & Thongam, K. (2020). RETRACTED ARTICLE: Computer-aided detection of brain tumor from magnetic resonance images using deep learning network. *Journal of Ambient Intelligence and Humanized Computing, 12*, 6911 - 6922.

[12]. Muhammad, K., Khan, S., Ser, J.D., & de Albuquerque, V.H. (2020). Deep Learning for Multigrade Brain Tumor Classification in Smart Healthcare Systems: A Prospective Survey. *IEEE Transactions on Neural Networks and Learning Systems, 32*, 507-522.

[13]. Sinha, S., Saraswat, A., & Bansal, S.A. (2022). Evaluation of Deep Learning Approaches for Detection of Brain Tumours using MRI. *2022 4th International Conference on Artificial Intelligence and Speech Technology (AIST)*, 1-5.

[14]. Kaur, D., Ummat, A., & Kaur, S. (2021). Comparative Study of Machine Learning Based Tumor Detection Techniques in Human Brain. *2021 2nd International Conference on Computational Methods in Science & Technology (ICCMST)*, 118-122.

[15]. Serra, J.J. (2021). Computed Tomography and Magnetic Resonance Imaging.

[16]. Raj, R.J., Shobana, S., Pustokhina, I.V., Pustokhin, D.A., Gupta, D., & Shankar, K. (2020). Optimal Feature Selection-Based Medical Image Classification Using Deep Learning Model in Internet of Medical Things. *IEEE Access, 8*, 58006-58017.

[17]. Islam, K.T., Ali, S., Miah, S., Rahman, M., Alam, S., & Hossain, M.A. (2021). Brain tumor detection in MR image using superpixels, principal component analysis and template based K-means clustering algorithm.

[18]. Shah, H.A., Saeed, F., Yun, S., Park, J., Paul, A., & Kang, J. (2022). A Robust Approach for Brain Tumor Detection in Magnetic Resonance Images Using Finetuned EfficientNet. *IEEE Access, PP*, 1-1.

[19]. Methil, A.S. (2021). Brain Tumor Detection using Deep Learning and Image Processing. *2021 International Conference on Artificial Intelligence and Smart Systems (ICAIS)*, 100-108.

[20]. Wang, P., & Chung, A.C. (2021). Relax and focus on brain tumor segmentation. *Medical image analysis, 75*, 102259.

[21]. Preethi, S., & Aishwarya, P. (2021). An efficient wavelet-based image fusion for brain tumor detection and segmentation over PET and MRI image. *Multimedia Tools and Applications, 80*, 14789 - 14806.

[22]. Overcast, W.B., Davis, K.M., Ho, C.Y., Hutchins, G.D., Green, M.A., Graner, B., &

Veronesi, M.C. (2021). Advanced imaging techniques for neuro-oncologic tumor diagnosis, with an emphasis on PET-MRI imaging of malignant brain tumors. *Current Oncology Reports, 23*.

[23]. Ramprasad, M.V., Rahman, M.Z., & Bayleyegn, M.D. (2022). A Deep Probabilistic Sensing and Learning Model for Brain Tumor Classification With Fusion-Net and HFCMIK Segmentation. *IEEE Open Journal of Engineering in Medicine and Biology, 3*, 178 - 188.

[24]. Ahmad, B., Sun, J., You, Q., Palade, V., & Mao, Z. (2022). Brain Tumor Classification Using a Combination of Variational Autoencoders and Generative Adversarial Networks. *Biomedicines, 10*.

[25]. Kang, J., Ullah, Z., & Gwak, J. (2021). MRI-Based Brain Tumor Classification Using Ensemble of Deep Features and Machine Learning Classifiers. *Sensors (Basel, Switzerland), 21*.

[26]. Nawaz, S.A., Khan, D.M., & Qadri, S. (2022). Brain Tumor Classification Based on Hybrid Optimized Multi-features Analysis Using Magnetic Resonance Imaging Dataset. *Applied Artificial Intelligence, 36*.

[27]. Yadav, A.S., Kumar, S., Karetla, G.R., Cotrina-Aliaga, J.C., Arias-Gonzáles, J.L., Kumar, V., Srivastava, S., Gupta, R., Ibrahim, S., Paul, R., Naik, N., Singla, B., & Tatkar, N.S. (2022). A Feature Extraction Using Probabilistic Neural Network and BTFSC-Net Model with Deep Learning for Brain Tumor Classification. *Journal of Imaging, 9*.

[28]. Ahuja, S., Panigrahi, B.K., & Gandhi, T.K. (2021). Enhanced performance of Dark-Nets for brain tumor classification and segmentation using colormap-based superpixel techniques. *Machine Learning with Applications*.

[29]. Amin, J., Sharif, M., Gul, N., Yasmin, M., & Shad, S.A. (2020). Brain tumor classification based on DWT fusion of MRI sequences using convolutional neural network. *Pattern Recognit. Lett., 129*, 115-122.

[30]. Aamir, M., Rahman, Z., Dayo, Z.A., Abro, W.A., Uddin, M.I., Khan, I., Imran, A.S., Ali, Z., Ishfaq, M., Guan, Y., & Hu, Z. (2022). A deep learning approach for brain tumor classification using MRI images. *Computers and Electrical Engineering*.

[31]. Amin, J., Sharif, M., Yasmin, M., & Fernandes, S.L. (2017). A distinctive approach in brain tumor detection and classification using MRI. *Pattern Recognit. Lett., 139*, 118-127.

[32]. Muezzinoglu, T., Baygin, N., Tuncer, I., Barua, P.D., Baygin, M., Dogan, S., Tuncer, T., Palmer, E., Cheong, K.H., & Acharya, U.R. (2023). PatchResNet: Multiple Patch Division–Based Deep Feature Fusion Framework for Brain Tumor Classification Using MRI Images. *Journal of Digital Imaging*, 1-15.

[33]. Sharif, M., Li, J.P., Amin, J., & Sharif, A. (2021). An improved framework for brain tumor analysis using MRI based on YOLOv2 and convolutional neural network. *Complex & Intelligent Systems, 7*, 2023 - 2036.

[34]. Tandel, G.S., Balestrieri, A., Jujaray, T., Khanna, N.N., Saba, L., & Suri, J.S. (2020). Multiclass magnetic resonance imaging brain tumor classification using artificial intelligence paradigm. *Computers in biology and medicine, 122*, 103804 .

[35]. Aamir, M., Rahman, Z., Abro, W.A., Bhatti, U.A., Dayo, Z.A., & Ishfaq, M. (2023). Brain tumor classification utilizing deep features derived from high-quality regions in MRI images. *Biomed. Signal Process. Control., 85*, 104988.

[36]. Kolla, M., Mishra, R., Zahoor Ul Huq, S., Vijayalata, Y., Gopalachari, M.V., & Siddiquee, K.N. (2022). CNN-Based Brain Tumor Detection Model Using Local Binary Pattern and Multilayered SVM Classifier. *Computational Intelligence and Neuroscience, 2022*.

[37]. Nayan, A., Mozumder, A.N., Haque, M.R., Sifat, F.H., Mahmud, K.R., Azad, A.K., & Kibria, M.G. (2022). A deep learning approach for brain tumor detection using magnetic resonance imaging. *ArXiv, abs/2210.13882*.

[38]. Rammurthy, D., & Mahesh, P.K. (2020). Whale Harris hawks optimization based deep learning classifier for brain tumor detection using MRI images. *Journal of King Saud University - Computer and Information Sciences*.

[39]. Raja, P.M., & rani, A.V. (2020). Brain tumor classification using a hybrid deep autoencoder with Bayesian fuzzy clustering-based segmentation approach. *Biocybernetics and Biomedical Engineering, 40*, 440-453.

[40]. Haubold, J., Demircioğlu, A., Gratz, M., Glas, M., Wrede, K.H., Sure, U., Antoch, G., Keyvani, K., Nittka, M., Kannengießer, S.D., Gulani, V., Griswold, M.A., Herrmann, K., Forsting, M., Nensa, F., & Umutlu, L. (2019). Non-invasive tumor decoding and phenotyping of cerebral gliomas utilizing multiparametric 18F-FET PET-MRI and MR Fingerprinting. *European Journal of Nuclear Medicine and Molecular Imaging, 47*, 1435 - 1445.